Inorganic Chemistry

Article

pubs.acs.org/IC

Dinuclear Rhenium Complexes as Redox-Active Pendants in a Novel Electrodeposited Polycyclopentadithiophene Material

Elsa Quartapelle Procopio,[†] Valentina Bonometti,[†] Monica Panigati,*[,†,‡] Pierluigi Mercandelli,*[,†,‡] Patrizia R. Mussini,*[,†,‡,§] Tiziana Benincori,[⊥] Giuseppe D'Alfonso,[†,‡] and Francesco Sannicolò[†,§]

[†]Dipartimento di Chimica, Università degli Studi di Milano, via Golgi 19, 20133 Milano, Italy

[‡]Unità di Ricerca di Milano del Consorzio INSTM, via Golgi 19, 20133 Milano, Italy

[§]Centro Interdisciplinare Materiali e Interfacce Nanostrutturati, via Celoria 16, 20133 Milano, Italy

[⊥]Dipartimento di Scienza e Alta Tecnologia, Università degli Studi dell'Insubria, via Valleggio 11, 22100 Como, Italy

Supporting Information

ABSTRACT: The novel $[Re_2(\mu\text{-H})(\mu\text{-OOC-CPDT})(CO)_6(\mu\text{-3-Me-pydz})]$ complex (**1**; OOC-CPDT = 4*H*-cyclopenta[2,1-*b*:3,4-*b*′]dithiophene-4-carboxylate, 3-Me-pydz = 3-methylpyridazine) has been prepared and characterized by single-crystal X-ray diffraction, density functional theory (DFT), and time-dependent DFT computations, UV−vis absorption and emission spectroscopy, and cyclic voltammetry (CV). The measured properties indicate the lack of electronic communication in the ground state between the CPDT and the rhenium diazine moieties. Oxidative electropolymerization of **1**, achieved by repeated potential cycling (−0.4 to +1.0 V vs Fc^+/Fc, in acetonitrile) with different supporting electrolytes, on different electrodes, afforded an electroactive and stable metallopolymer (poly-**1**). In situ measurements of the mass of the growing film (on a gold electrode, with an electrochemical quartz microbalance) confirmed the regularity of the polymerization process. The polymer exhibits two reversible oxidation peaks of the thiophene chain and a broad irreversible reduction peak (−1.4 V, quite close to that observed for the reduction of monomer **1**), associated with a remarkably delayed sharp return peak, of comparable associated charge, appearing in close proximity (+0.3 V) to the first oxidation peak of the neutral polythiophene chain. This charge-trapping effect can be observed upon repeated cycles of p and n doping, and the negative charge is maintained even if the charged electrode is removed from the solution for many hours. Electrochemical impedance spectroscopy showed that the main CV oxidation peak corresponds to facile charge transfer, combined with very fast diffusion of both electrons and ions within the polymer. In summary, poly-**1** provides a new example of a metallopolymer, in which the conductive properties of the π-conjugated system are added to the redox behavior of the pendant-isolated complexes.

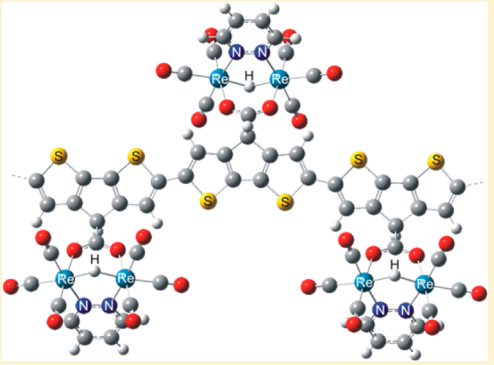

INTRODUCTION

Many efforts have been devoted to incorporating metal centers in conjugated polymers, pointing toward expanding functionalities and performances in many fields, such as sensing,[1] catalysis,[2] photovoltaics,[3] electroluminescence,[4] information storage,[5] and electrochromism.[6] To tune the properties of the metallopolymers, different metal centers have been used, from transition to main-group metals to lanthanides.[7] Moreover, different metal−polymer linkages have been exploited, ranging from strong covalent bonds to more labile coordination interactions, resulting in "static" or "dynamic" binding modes.[8]

The metal centers have been either incorporated into the conducting skeleton, with strong coupling between the metal orbitals and those of the π-conjugated system, or bonded as pendants of the polymer chain.[7e,9] In this arrangement, the metal complexes are not involved in the p conductivity of the backbone but can make available a parallel conduction pathway, through an "outer-sphere" charge-transfer mechanism, provided they have redox properties.[7e,9] Moreover, the geometric and steric constraints of the metal complexes can orient the π-conjugated materials into specific solid-state arrangements, affecting their conductivity properties.

Many synthetic routes to metallopolymers have been developed. The electrochemical polymerization of monomers containing transition-metal complexes[10] has been used for functionalized fluorene or vinylene monomers or for monomers containing nitrogen heterocycles, while only a few examples concerned thiophenes functionalized with substituents capable of anchoring transition metals (usually polypyridines, as ligands for ruthenium, iron, platinum, and, in very few cases, rhenium).[11,7e,g]

We report here the characterization of a new metallopolymer obtained by electropolymerization of the dinuclear hydridocarbonylrhenium(I) complex $[Re_2(\mu\text{-H})(\mu\text{-OOC-CPDT})(CO)_6(\mu\text{-3-Me-pydz})]$ (**1**, Chart 1), where 3-Me-pydz

Received: July 29, 2014
Published: October 6, 2014

   dx.doi.org/10.1021/ic501840p | *Inorg. Chem.* 2014, 53, 11242−11251

Chart 1. Chemical Structure of 1

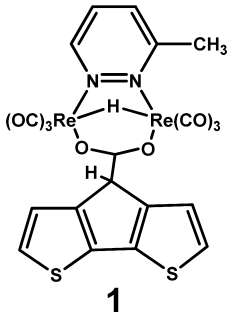

1

indicates 3-methylpyridazine and CPDT the 4*H*-cyclopenta-[2,1-*b*;3,4-*b*′]dithiophene-4-yl group. The CPDT system was chosen for its very high polymerogenic ability, independent of the bulkiness of the substituents in position 4, and for the generally high stability of the resulting polymers.[12] Moreover, CPDT-based materials display a wide range of interesting physical properties, including high electrical conductivity, low band gap, and extended π conjugation. In addition, it is possible to functionalize these materials because a wide range of groups can be bonded in the 4 position, allowing one to tune the properties of the material. In 1995, Zotti et al. reported the preparation and electropolymerization of cyclopentadithiophenes carrying redox centers, such as ferrocene groups.[13] Examples are also known of CPDT polymers containing a ruthenium(II) phenanthroline complex hanging on a CPDT backbone.[14]

The dinuclear rhenium complex anchored to the CPDT backbone belongs to a family of neutral carbonylrhenium(I) complexes with the general formula $[Re_2(\mu\text{-}X)_2(CO)_6(\mu\text{-}1,2\text{-diazine})]$, where X can be halogen,[15] hydride,[16] or alkoxide or thiophenoxide.[17] Some of them have recently gained interest for their intense yellow/green emission, occurring from triplet metal-to-ligand charge-transfer (^{3}MLCT) states, showing the modulation effect of the diazine substituents on energy, lifetimes, and quantum yields of the emission.[18] These properties allowed their successful use as phosphorescent dopants in organic light-emitting devices.[19,20] A distinctive feature of this class of complexes is the relatively low-lying lowest unoccupied molecular orbital (LUMO) level, localized on the bridging diazine ligand. Here this feature has been exploited to obtain, by electroplymerization of **1**, a material that joins the conductive properties of a thiophene polymer to the easy reducibility of the pendant complex.

RESULTS AND DISCUSSION

Synthesis and Characterization of the Monomer 1. The starting material was the electronically unsaturated (32 valence electrons) dinuclear hydridocarbonyl complex $[Re_2(\mu\text{-}H)_2(CO)_6(\mu\text{-}3\text{-Me-pydz})]$ (**2**, Scheme 1), obtained by reaction of the unsaturated tetranuclear hydridocarbonyl cluster $[Re_4(\mu_3\text{-}H)_4(CO)_{12}]$ with 2 equiv of 3-Me-pydz.[16] Dihydrido complexes like **2** can be easily functionalized, owing to their high reactivity toward acid molecules. This reactivity was exploited to connect a COOH-functionalized CPDT molecule to the dinuclear rhenium moiety (Scheme 1). The treatment of **2** with a slight excess of CPDT-COOH (toluene, reflux, 32 h) resulted in H_2 evolution and coordination of the CPDT-containing fragment through the carboxylate anion. The ^{1}H NMR spectrum showed, besides the pyridazine signals, one hydride resonance (δ −6.80 ppm) and the expected five resonances of the CPDT moiety due to the C_1 symmetry of **1**. Crystals of **1** suitable for X-ray analysis were obtained by the slow diffusion of *n*-hexane (−25 °C) into a saturated CH_2Cl_2 solution.

Scheme 1. Synthesis of Monomer 1

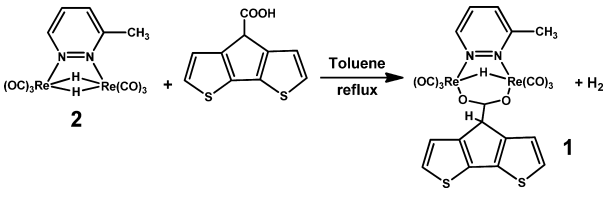

Solid-State Structure. The structure of the complex has been determined by single-crystal X-ray analysis. Figure 1 shows frontal and lateral views of the molecule. In this dinuclear species, each rhenium atom attains a distorted octahedral coordination and bears three terminal carbonyl ligands in a facial arrangement, one of the nitrogen atoms of the bridging pyridazine ligand, a bridging hydrido ligand, and one of the two oxygen atoms of the bridging 4*H*-cyclopenta[2,1-*b*:3,4-*b*′]dithiophene-4-carboxylato ligand. Because of the presence of the methyl substituent on the pyridazine, the molecule is overall asymmetrical. This asymmetry is particularly evident in the skewed conformation adopted by the CPDT-carboxylato ligand, as measured by the H(1)···C(8)−C(34)−H(34) torsional angle of 145.0° (in a symmetrical structure, it should be 0° or 180°). This conformation maximizes the intramolecular distance between the pyridazine and cyclopentadithiophene rings. However, the main structural motif observed in the crystal is the $\pi-\pi$ stacking between the pyridazine and cyclopentadithiophene rings of two adjacent molecules (see Figure S1 in the Supporting Information, SI).

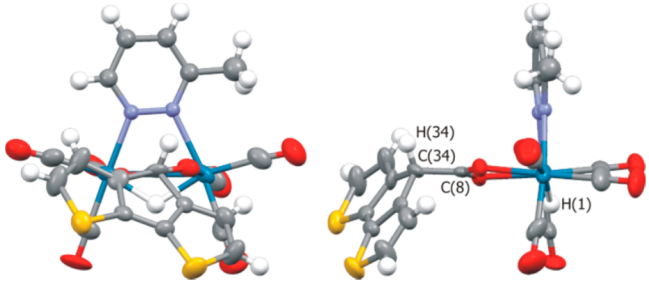

Figure 1. Frontal and lateral views of **1** with a partial labeling scheme. Only the major component of the disordered 3-methylpyridazine ligand is depicted. Displacement ellipsoids are drawn at the 50% probability level. Hydrogen atoms are given arbitrary radii. Color code: C, gray; H, white; N, blue; O, red; Re, teal; S, yellow.

Computational Study. The new rhenium complex **1** was studied by means of density functional theory (DFT) and time-dependent DFT (TD-DFT) computations. Two optimized structures have been found, differing in the rotation of the cyclopentadithiophene substituent around the C(8)−C(34) bond. One of them is similar to the conformer observed in the solid state, having an H(1)···C(8)−C(34)−H(34) torsional angle of 161.4°; the other one (more stable by 6.9 kJ mol^{-1}) shows a closer arrangement of the pyridazine and cyclopentadithiophene rings and has a torsional angle of −12.8° (see Figure S2 in the SI). The torsional barrier for their interconversion is computed to be as low as 8.0 kJ mol^{-1},

dx.doi.org/10.1021/ic501840p | Inorg. Chem. 2014, 53, 11242−11251

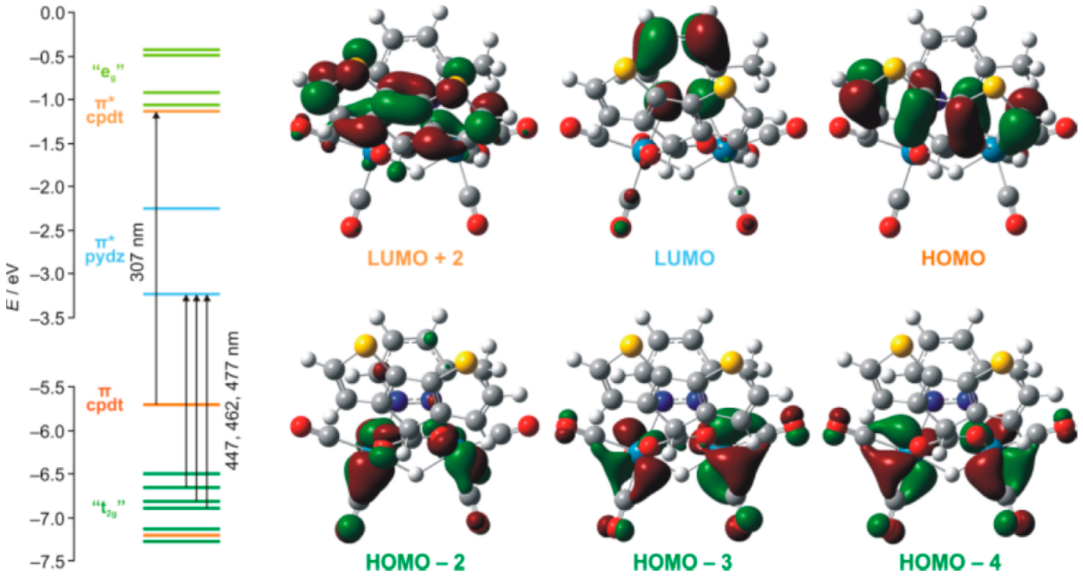

Figure 2. Partial MO diagram for complex **1**. Orbitals are colored according to their main contribution: rhenium "t_{2g}" orbitals (dark green), cyclopentadithiophene π orbitals (orange), pyridazine π^* orbitals (light blue), rhenium "e_g" orbitals (light green), and cyclopentadithiophene π^* orbitals (light orange). Arrows correspond to electronic transitions involved in the absorption spectra (computed TD-DFT wavelengths are given). In particular, values on the left and on the right refer to the cyclopentadithiophene $\pi-\pi^*$ and MLLCT absorptions, respectively. Some relevant MOs are depicted (isovalue = 0.04 au).

suggesting that free rotation occurs at room temperature. This can be explained by the strongly asymmetrical arrangement of the carbonyl ligands that, because of the different size of the bridging hydrido and carboxylato ligands, leave one side of the complex almost unhindered (see Figure 1).

Orbital energies and absorption wavelengths computed for the two rotamers are qualitatively similar, and only the ones for the more stable conformation are discussed (data can be found in Tables S1 and S2 in the SI). A partial orbital energy diagram is depicted in Figure 2, along with some relevant molecular orbital (MO) plots.

The highest occupied molecular orbital (HOMO) is the highest-lying π orbital of the cyclopentadithiophene group. Lower in energy lie six orbitals corresponding to the "t_{2g}" set of the two rhenium atoms in a pseudooctahedral environment. In particular, three of them show a strong rhenium μ-carboxylato π^* character, in close analogy with the derivatives previously described.[15,17] As is typical for these species, LUMO and LUMO+1 are the two lowest-lying π^* orbitals of the coordinated pyridazine. LUMO+2 is the lowest-lying π^* orbital of the cyclopentadithiophene group, while the following four MOs are the "e_g" set of the two rhenium atoms (showing in addition a large C≡O π^* character).

The absorption spectrum down to 270 nm was simulated by computing the lowest 30 singlet excitation energies. Selected transitions are depicted in Figure 2. The absorptions starting from the rhenium "t_{2g}" orbitals can be described as metal−ligand-to-ligand charge-transfer (^{1}MLLCT) transitions, taking into account the significant contribution of the bridging ancillary ligands to the metal-centered HOMO set. The three more intense transitions (from HOMO−n to LUMO) are listed in Figure 2 and Table S2 in the SI.

Photophysical Characterization of 1. The absorption spectra of complex **1** and CPDT-COOH ligand are shown in Figure 3. On the basis of DFT computations, the lowest-energy absorption of the complex, at 413 nm, can be assigned to the convolution of multiple ^{1}MLLCT transitions. The charge-transfer character of such transitions is supported by their strong solvent dependence: indeed, as was already reported for the related dirhenium μ-diazine complexes,[18] a blue shift is observed upon increasing solvent polarity (see Figure S3 in the SI).

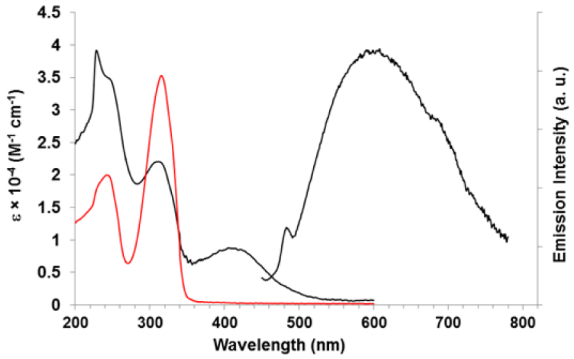

Figure 3. Black lines: absorption and emission spectra of **1** in a deaerated dichloromethane solution at room temperature. Red line: absorption spectrum of the free CPDT-COOH ligand under identical conditions.

The position of the two absorptions of the CPDT-COOH ligand, arising from $\pi-\pi^*$ transitions of the thiophene system,[21] did not show significant changes upon complexation, indicating that the CPDT π system does not significantly interact with the Re_2-pydz orbitals. The change of the relative intensities can be attributed to a partial overlap between the highest-energy band of the ligand and the d−d transitions of the $Re_2(\mu\text{-}X)_2(CO)_6$ moiety.[17,18]

Upon excitation at 450 nm, complex **1** exhibits weak photoluminescence, centered at 607 nm, attributed to the emission from ^{3}MLCT excited states (Figure 3), typical of this class of complexes.[18] The photoluminescence quantum yields of **1** (Φ = 0.05%) are lower than those of related $[Re_2(\mu\text{-H})(\mu\text{-OR})(CO)_6(\mu\text{-3-Me-pydz})]$ complexes (Φ = 0.55% and 0.07% for R = Ph and Me, respectively).[22] This might be due to the

dx.doi.org/10.1021/ic501840p | Inorg. Chem. 2014, 53, 11242−11251

lower stiffness of the $Re_2(\mu\text{-H})(\mu\text{-X})$ scaffold, with X is bridging through two donor atoms rather than one (Re−O−C−O−Re instead of Re−O−Re).

Electrochemical Characterization of 1. Cyclic voltammetry (CV) was employed for the characterization of **1**, for its anodic polymerization, and for the characterization of the resulting polymer. The normalized CV pattern of **1**, recorded on a glassy carbon (GC) electrode, in MeCN with 0.1 M $TBAPF_6$ (TBA = NBu_4) as the supporting electrolyte, is reported in Figure 4. For comparison, the CV patterns of the

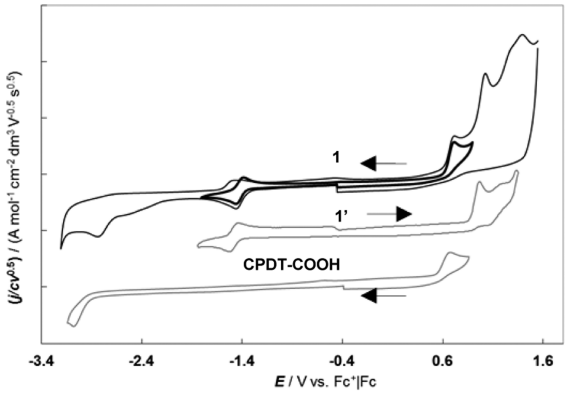

Figure 4. Normalized CV patterns, recorded on GC, at 0.2 V s^{-1} in MeCN with a 0.1 M $TBAPF_6$ medium (starting from −0.4 V vs Fc^+/Fc), for complex **1** together with reference compounds **1′** and CPDT-COOH.

corresponding free ligand CPDT-COOH and of the related rhenium complex $[Re_2(\mu\text{-H})(\mu\text{-OOC-Ph})(CO)_6(\mu\text{-3-Me-pydz})]$ (**1′**),[22] which contains one hydride and one benzoate anions as ancillary ligands, are also reported. The peak and onset potentials, together with the related HOMO and LUMO energies, calculated as previously described,[23] are collected in Table 1. It is worthwhile to notice that the HOMO−LUMO energy gap calculated from the electrochemical experiment (2.16 eV, max, or 1.93 eV, onset) is much narrower than the energy gap calculated from the lowest-energy UV−vis absorption peak (3.01 eV, max). This is consistent with the fact that the electronic absorption arises from a ^{1}MLLCT transition, which does not involve the HOMO level (π-CPDT; see the previous section).

The first oxidation peak of **1** at 0.71 V vs Fc^+/Fc (chemically irreversible) can be assigned, by comparison with CPDT-COOH, to the formation of a radical cation delocalized over the cyclopentadithiophene moiety.[24] The second oxidation peak at +1.02 V vs Fc^+/Fc corresponds to oxidation of the binuclear rhenium core, by comparison with the behavior of the model complex **1′** (see Table 1). On the other hand, the first reduction peak of **1**, located at −1.45 V (Fc^+/Fc), is nearly coincident with that of **1′**, both in position and in shape. In agreement with many related dirhenium pyridazine complexes,[18] the reduction of **1** and **1′** is monoelectronic and reversible, both chemically (symmetrical return peaks, independent of the scan direction) and electrochemically (facile electron transfer, which is indicated by the 57 mV half-peak widths and the almost-zero E_p vs log ν slopes). This agrees with the very fast formation of a stable radical anion.

Therefore, the CV features of **1** confirm that the HOMO is localized on the CPDT unit and the LUMO essentially consists of the π^* orbitals of the pyridazine ligand, in agreement with the DFT computations. Moreover, the values of the oxidation and reduction potentials, very similar to those observed in free CPDT-COOH and in the model complex **1′**, confirm the lack of communication between the pyridazine ring and the CPDT moiety, consistent with the indications of UV−vis absorption data (see the previous section).

Electropolymerization. Regular oxidative electropolymerization of monomer **1** was achieved by repeated potential cycles between −0.4 and +1.0 V vs Fc^+/Fc, in MeCN, with different supporting electrolytes, on different electrodes [GC, platinum, gold, and indium-doped tin oxide (ITO)]. Sequential cyclic voltammograms of **1** (Figure 5a) gave evidence that the polymer films remain highly electroactive during the polymerization process: oxidative and reductive peak currents regularly increased with no apparent threshold (very regular growth was observed even up to 60 cycles; see Figure S4 in the SI).

The sequential cyclic voltammograms of free CPDT-COOH, recorded under similar conditions (Figure 5b), showed that the two monomers have a comparable polymerization ability. Therefore, the binding of the CPDT moiety to the metal complex does not significantly hamper its oxidative coupling, in spite of the bulkiness of the organometallic fragment.

The two polymerization patterns are similar, which is reasonable, considering that polymerization involves the same α positions available in the CPDT unit in both cases. In particular, both show two large, reversible peaks, the first one smaller than the second one, at 0.2 V s^{-1} scan rate. Such reversible peaks are particularly well-defined and symmetrical in the case of **1**, pointing to an easy solid-state charging/uncharging process.

The stability of the poly-**1** films was tested by transferring the carefully rinsed polymer-modified electrodes into a monomer-free solution and by performing repeated oxidative cycles around the first two oxidation peaks, as shown in Figure S5 in the SI. The polymers exhibited remarkable stability, and their CV characteristics remained almost unchanged even upon prolonged cycling.

These general features were observed in all operating conditions, albeit small differences in the polymer CV patterns

Table 1. Oxidation and Reduction Peak and Onset Potentials, Referring to the Fc^+/Fc Couple, and Related HOMO and LUMO Values, for the Monomer 1 Together with the Reference Molecules 1′ and CPDT-COOH

	reduction peak/V (Fc^+/Fc)		oxidation peak(s)/V (Fc^+/Fc)				energy levels and gaps/eV					
							onset			max		
	max	onset	onset	max	onset	max	LUMO	HOMO	E_g	LUMO	HOMO	E_g
CPDT-COOH	−3.08	−2.88	0.52	0.67			−1.92	−5.32	3.40	−1.72	−5.47	3.75
1′	−1.52	−1.42			0.86	0.97	−3.38	−5.66	2.28	−3.28	−5.77	2.49
1	−1.45	−1.34	0.59	0.71		1.02	−3.46	−5.39	1.93	−3.35	−5.51	2.16

dx.doi.org/10.1021/ic501840p | Inorg. Chem. 2014, 53, 11242−11251

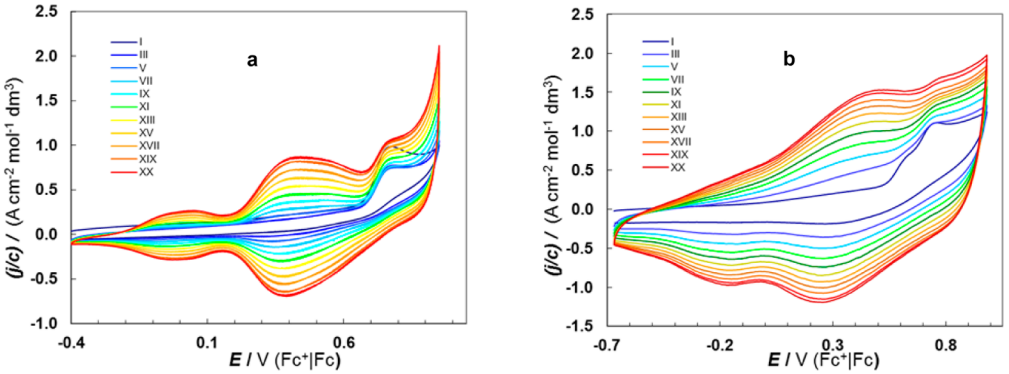

Figure 5. Oxidative electropolymerization of (a) monomer **1** (0.5 mM, MeCN, 0.1 M $TBAPF_6$) performed on a GC electrode by potential cycling between −0.4 and 1.0 V vs Fc^+/Fc (0.2 V s^{-1}) and of (b) CPDT-COOH (0.5 mM), performed under similar conditions, with potential cycling between −0.66 and 0.94 V. The Roman numerals indicate the number of potential cycles.

were observed, changing the supporting electrolyte, the electrode substrate, and/or the width of the potential range for the polymerization cycles (examples are provided in Figures S4, S6, and S7 in the SI); in particular, a narrower potential range resulted in a slower film growth because of the reduced interval time and the lower conversion of monomer within this potential window.

The oxidative CV pattern of poly-**1**, similar to that of other cyclopentadithiophene polymers,[5,25,26] is characterized by the two reversible thiophene oxidation peaks observed in the electropolymerization process.

The regularity of the polymerization can be finely appreciated by measuring in situ the weight mass of the growing film on gold electrodes with an electrochemical quartz microbalance (EQCM; Figure 6). The weight of the forming

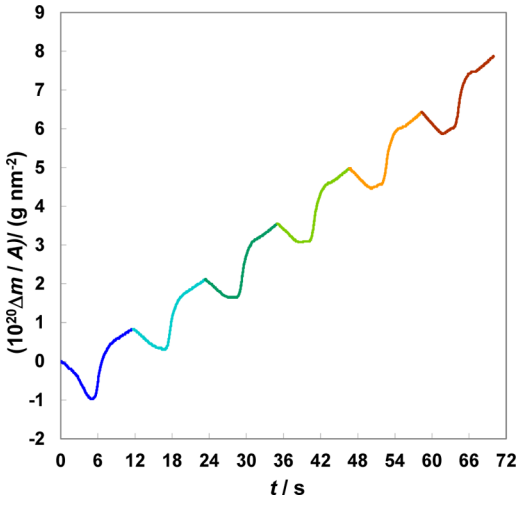

Figure 6. EQCM monitoring (as mass variation per active surface area, cycles I–VI) of the electropolymerization of monomer **1** on gold (0.25 mM in MeCN and 0.1 M $TBAPF_6$ at 0.2 V s^{-1}).

polymer (monitored from the decrease of the frequency of the quartz oscillator supporting the gold electrode; see the lower section of Figure S8a in the SI) increased linearly with time (Figure S8b in the SI), with a periodic fine structure corresponding to the ingress/egress of ions and solvent within each cycle.

Charge Trapping. After the poly-**1** stability was tested at positive potentials, the potential scan range was widened toward more negative values, revealing a broad irreversible reduction peak at −1.4/−1.5 V (vs Fc^+/Fc, with the onset being at −1.1/−1.2 V; Figure 7). The potential value, quite close to that observed for the reduction of monomer **1**, indicates that the negative charge is injected into the π^* orbitals of the diazine units.[27]

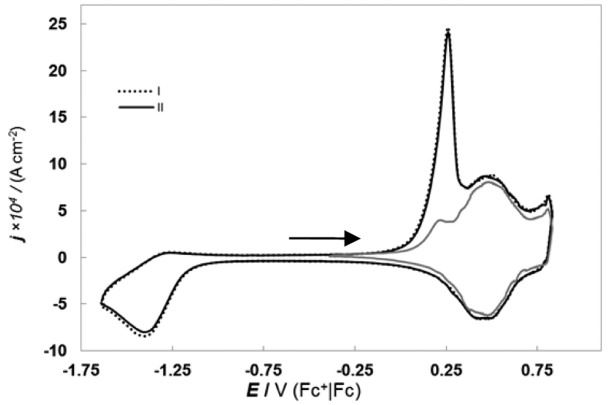

Figure 7. CV traces showing the charge-trapping phenomenon, recorded at 0.2 V s^{-1} in a monomer-free solution, on a film obtained from a 60-cycle electropolymerization of monomer **1** on GC, in a MeCN and 0.1 M $TBABF_4$ medium. For comparison, the gray curve provides a typical stability cycle of the same film in a monomer-free solution, limiting the potential scan to the reversible oxidation region.

The reduction peak is associated with a remarkably delayed sharp return peak, of comparable area (i.e., associated charge), appearing in close proximity to the first oxidation peak of the neutral polythiophene chain. This behavior has been observed in all of the experiments involving poly-**1**, using different supporting electrolytes, and on all of the tested electrode surfaces, and it is consistent with the presence of a solid-state charge-trapping phenomenon, implying that the negative charge, injected at a given cathodic potential, is recovered at much higher potentials in the reverse scan.[28]

Charge trapping, a typical property of electroactive materials bearing electron-rich and -poor moieties, can be explained by invoking different processes, depending on the molecular structures and the working conditions involved. Indeed, the higher than expected reoxidation potential can be ascribed to a strong stabilization of the reduced species[29] or to some conformational changes of the film components[30] (concurrent with the ingress or egress of ions and solvent molecules),

dx.doi.org/10.1021/ic501840p | Inorg. Chem. 2014, 53, 11242−11251

resulting in a more stable supramolecular structure. Such changes could result in kinetic barriers to the efficient reuptake of the ejected species (or to the egress of the entered species) upon reoxidation, which can be overcome only by providing a significant energy supplement. On the other hand, charges created upon reduction can become trapped in isolated microdomains in the insulating film; therefore, they can be too immobile or too dilute to allow charge transfer to the electrode. These charges can be released only when the film is scanned positive enough to begin oxidation of the backbone, becoming conductive and thus able to mediate electron transfer.[31,32]

In our case, the assumption of a supramolecular reorganization is supported by the observation that the amount of charge associated with the reduction and the charge-trapping process regularly decreases with increasing scan rates, pointing to a somehow slow solid-state process occurring at the first reduction peak, concurrently with charge transfer (Figure 8).[29]

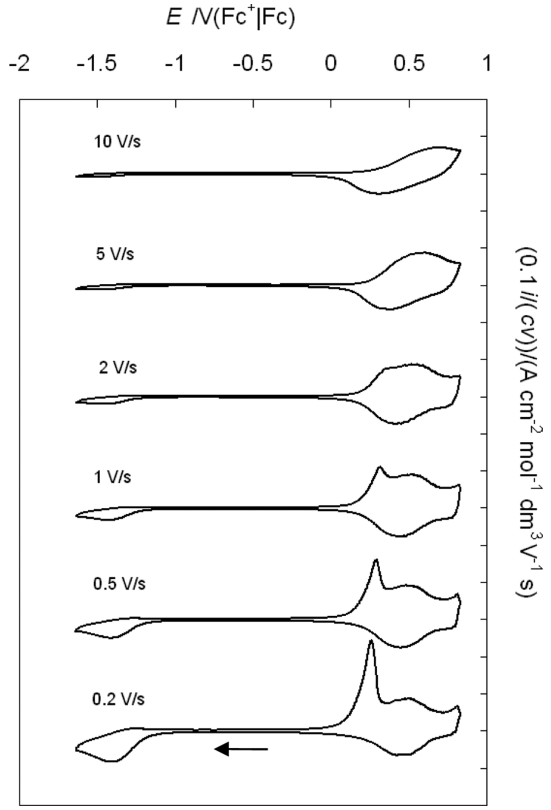

Figure 8. CV cycles including the charge-trapping phenomenon, recorded at different scan rates on a film obtained from a 60-cycle electropolymerization of monomer **1** on GC, in MeCN and 0.1 M $TBABF_4$ medium, starting from −0.4 V and scanning the cathodic region before.

In any case, this effect appears to be quite interesting, in many terms. At sufficiently low scan rates, the associated charge is high, almost comparable to the charge generated in polymer oxidation. Moreover, the charges associated with the forward and backward charge-trapping peaks are comparable, pointing to the fact that the entire negative charge is firmly trapped until the first oxidation peak is attained. Furthermore, the charge-trapping process is reversible upon repeated cycling of p and n doping, showing that the polymer network is undamaged by this process. Finally, a negative charge is maintained (and released upon oxidation) even if the negatively charged electrode is removed from the solution and stored for many hours (for instance, overnight) at room temperature.

3.8. Electrochemical Impedance Spectroscopy (EIS). The film was also studied in a monomer-free solution by comparing its electrochemical impedance at different potentials as representative of different possible states. Figure 9 provides a synopsis of the relevant Nyquist, Bode modulus, and Bode phase diagrams.

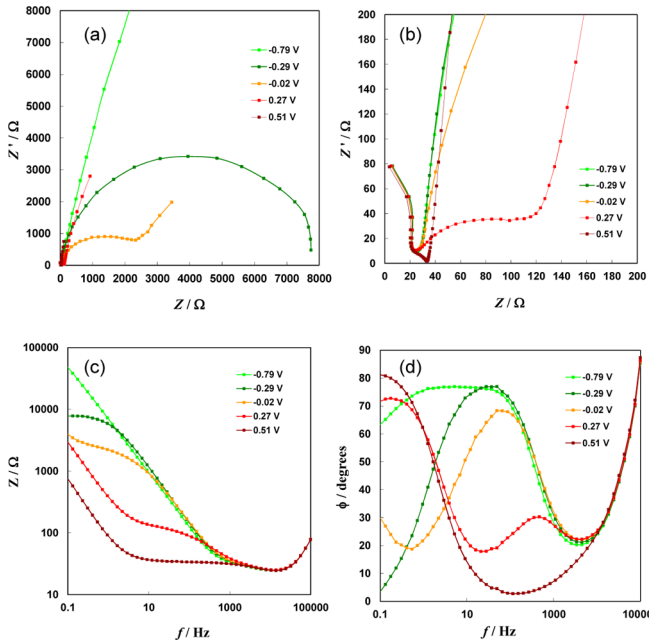

Figure 9. EIS features of the conducting film obtained by 20-cycle electropolymerization of 0.25 mM monomer **1** on a GC electrode, in a MeCN and 0.1 M $TBAPF_6$ medium, at 0.2 V s^{-1}: (a and b) Nyquist phase diagrams of the imaginary versus real components of the impedance *Z*, focusing on medium and high frequencies, respectively; (c) Bode modulus phase diagram; (d) Bode phase diagram.

At −0.79 V vs Fc^+/Fc, poly-**1** is in its neutral state (see Figure 8), far away from both its oxidation and reduction potentials. Accordingly, it exhibits purely capacitive behavior (corresponding to a nearly vertical line from high to low frequencies in the Nyquist phase diagram and a nearly 90° asymptote in the Bode phase diagram).

At sufficiently positive potentials to allow charge transfer from the polymer to the electrode, changes are observed in the shapes of the curves, in both the Nyquist and Bode diagrams, which can be rationalized in terms of the nature of the rate-determining steps at the different frequencies, following the treatment described by Musiani (summarized in the SI).[33]

At more positive potentials than −0.79 V, the capacitive straight line is replaced in the Nyquist phase diagram at high frequencies (frequency decreases from left to right in the horizontal axis) by half-cycles of decreasing diameter, pointing to electron transfer as rds and decreasing charge-transfer resistance upon increasing potential. Thus, it can be observed that some electron transfer takes place already at −0.29 V, although it is kinetically very hindered and possibly corresponds to only a few reaction sites per surface unit ($R \approx 8000\ \Omega$; Figure 9a). Then, shifting to −0.02 V, electron transfer becomes easier, the half-circle diameter remarkably decreases ($R \approx 2300\ \Omega$; Figure 9a), and a small portion of the

dx.doi.org/10.1021/ic501840p | Inorg. Chem. 2014, 53, 11242−11251

Warburg straight line, with 45° slope,[34] can be perceived at the lowest frequencies. This implies the diffusion of charges (both electrons and ions) within the polymer to be kinetically determining. At 0.27 V, the charge-transfer resistance is dramatically lower ($R \approx 100\ \Omega$; Figure 9b); furthermore, the contiguous "diffusive" Warburg section is practically unnoticed, pointing to high conductivity (electronic and ionic) within the polymer. As a consequence, after the small *RC* semicircle, the system in the "charge saturation" state turns into a capacitive response with no apparent intermediate diffusive regimen. Finally, at 0.51 V the charge-transfer resistance is nearly unperceivable and the system soon reaches the capacitive behavior.

This indicates that the main CV oxidation peak corresponds to extremely facile charge transfer combined with very fast diffusion of both electrons and ions within the polymer. The good conductivity (both electronic and ionic) of the polymer was also revealed by the presence of the oxidation peak of monomer **1**, at about 0.71 V, in the CV traces recorded during the electropolymerization of **1** (see Figure 5a).

The decreasing charge-transfer resistance is also well recognized in the Bode modulus phase diagram (Figure 9c), in terms of horizontal plateau, providing the *R* values (with respect to the niveau associated with the electrolyte solution resistance); it gets lower and shifts to higher frequencies with increasing potential. It can also be recognized in the Bode phase diagram (Figure 9d), in terms of peaks, again shifting to higher frequencies with increasing potential.

Spectroelectrochemistry. The electrooptical properties of the films deposited onto ITO-coated glass electrodes in a MeCN solution (0.1 M $TBAPF_6$) have been investigated. At −0.39 V (vs Fc^+/Fc), the film is neutral. Accordingly, its UV−vis spectrum (Figure 10) shows a (partially overlapped) ^{1}MLLCT transition at 410 nm and a $\pi-\pi^*$ transition of the polythiophene backbone at 496 nm. The first band lies at the same energy as that of the band observed for monomer **1** (Figure 3) because the diazine ligands are not involved in the polymerization process and are not conjugated to the polymer backbone. On the contrary, the band due a $\pi-\pi^*$ transition shifts to longer wavelengths, with respect to the corresponding band in monomer **1**, and this red shift increases with the number of electropolymerization cycles (from 496 nm for 10 polymerization cycles, as in Figure 10, to 545 nm for 40 cycles), as a consequence of the π-conjugation extension.[21] This absorption maximum is at lower wavelength than that of the bulk polymer (600 nm),[13] suggesting a rather low degree of polymerization, as was previously observed for CPDT-COOH itself,[21] or other electropolymerized CPDT monomers carrying redox pendant groups.[35]

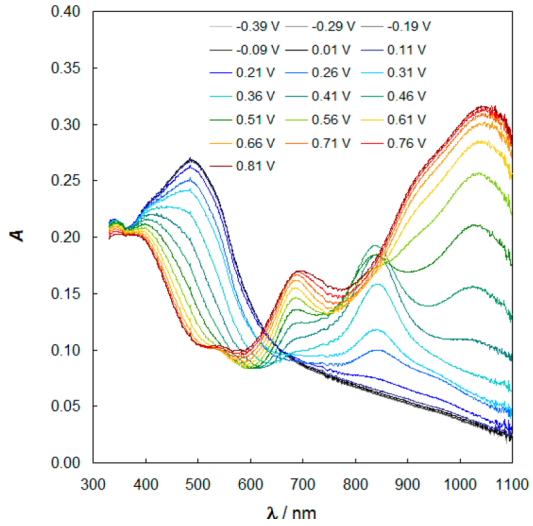

Figure 10. Spectroelectrochemistry of a film (10 polymerization cycles) of poly-**1** on ITO-coated glass (MeCN and 0.1 M $TBAPF_6$) at applied potentials between −0.39 and 0.81 V (vs Fc^+/Fc).

Upon a stepwise increase in the electrode potential up to 0.36 V, the absorption band of the polythiophene chain progressively disappears and a broad band emerges at 830 nm, attributable to the radical cation.[36] The ^{1}MLLCT band at 410 nm is still perceivable, in agreement with the electrochemical data, indicating that the metal core is not involved in backbone oxidation.

A further increase of the potential to 0.81 V results in the progressive growth of new absorption bands at 690, 900 (shoulder), and 1050 nm. The formation of a bipolaronic species should afford only one new absorption, at lower energy than the radical cation. Therefore, the presence of different absorptions, one of which is at higher energy, could be a hint of π dimerization of the polarons, which affords spinless bipolaronic species, stabilized with respect the two separated polarons.[37] According to the selection rules for the π dimer, three absorption bands (often overlapped) are expected, two of them at higher energy than the corresponding polaronic band.[36]

When the potential is settled at negative values (down to −1.4 V vs Fc^+/Fc, corresponding to the first reduction potential), no changes in the UV−vis spectrum of poly-**1** are observed, in agreement with the absence of electronic communication between the thiophene polymer backbone and pyridazine moieties.

CONCLUSIONS

A new dinuclear rhenium complex containing a cyclopentadithiophene moiety has been synthesized and fully characterized. At the molecular level, the spectroscopic and electrochemical properties of the complex result from the addition of the properties of two separate building blocks, namely, the CPDT-COOH and organometallic fragments, in agreement with the lack of electronic communication in the ground state between the two fragments, indicated by the DFT computations.

In spite of the steric hindrance of the dinuclear scaffold of the dirhenium complex, electropolymerization of the CPDT moiety does occur, on different electrodes, although with a low polymerization degree. The metallopolymer is constituted by a poly-CPDT conjugated chain, regularly decorated by pendant dirhenium diazine complexes (one complex for every CPDT group). It provides an example of a metallopolymer, in which the conductive properties of the π-conjugated system are added to the redox behavior of the pendant-isolated complexes. Easy charge injection and diffusion (both electrons and ions) within the polymer have been confirmed by EIS measurements. The good stability of the conductive polymer film on different electrodes, from GC to ITO to platinum and gold, has been indicated by its reproducible behavior upon repeated potential cycles.

In addition, poly-**1** exhibits not only the high p-doping stability typical of poly-CPDT but also a high n-doping stability

dx.doi.org/10.1021/ic501840p | *Inorg. Chem.* 2014, 53, 11242−11251

Scheme 2. Synthetic Approach to CPDT-COOH

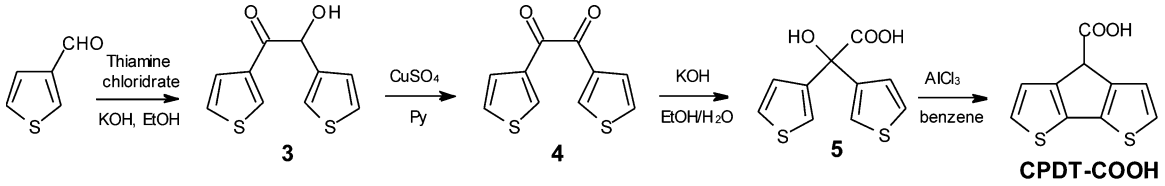

because of the presence of the electron-poor rhenium diazine groups, which are the site of reduction. The negative charge is removed at much higher potential than the reduction (ca. 1.7 V more positive), in concomitance with the onset of the p-doping process. Such a charge-trapping process can be observed upon repeated potential cycles, indicating that the polymer network is undamaged by the process. Notably, the negative charge is preserved even if the charged electrode is removed from the solution and stored overnight at room temperature. Possible applications for rewritable memory devices can be envisaged. Moreover, immobilization of the complex on a conductive film on an electrode surface will provide a favorable arrangement for testing in heterogeneous conditions the properties of dirhenium diazine complexes already ascertained in the homogeneous phase, such as the recently reported activity in the electrocatalytic reduction of carbon dioxide.[38]

EXPERIMENTAL SECTION

Materials and Instrumentation. All of the reactions were performed under dinitrogen using the Schlenk technique and solvents deoxygenated and dried by standard methods. 3-Methylpyridazine was used as received from Aldrich. $[Re_2(\mu\text{-}H)_2(CO)_6(\mu\text{-}3\text{-}Me\text{-}pydz)]$ (**2**),[16] and 4*H*-cyclopenta[2,1-*b*:3,4-*b*′]dithiophene-4-carboxylic acid (CPDT-COOH, Scheme 2)[39] were prepared according to literature methods. ^{1}H NMR spectra were recorded on a Bruker DRX300 or DRX400 spectrometer. IR spectra were acquired on a Bruker Vector22 FT instrument. Electronic absorption spectra were recorded on an Agilent 8543 spectrophotometer, at room temperature. Mass spectrometry by secondary-ion ionization were recorded using a VG AUTOSPEC M246 magnetic spectrometer using 3-nitrobenzyl alcohol as the matrix.

Synthesis of CPDT-COOH. CPDT-COOH was obtained by benzoinic condensation of 3-thiophenecarboxyaldehyde, mediated by thiamine chlorohydrate in ethanol, at pH 9 following a modified literature procedure.[40] Control of the pH has a crucial role in the reaction because thiamine chlorohydrate is inactive at lower or higher values. It is worth noting that the pH decreases constantly during the reaction; therefore, continual KOH addition is necessary. The resulting 3,3′-thienoin **3** was oxidized with copper sulfate to give the 3,3′-thienyl **4**, which, in the presence of KOH, underwent benzylic transposition to give the hydroxyl acid **5**. CDPT-COOH resulted then from intramolecular Friedels-Crafts-type ring closure, promoted by $AlCl_3$ in benzene.

Synthesis of Complexes 1 and 1′. A mixture of **2** (39.8 mg, 0.0625 mmol) and CPDT-COOH (16.9 mg, 0.0750 mmol, 1.2 equiv) was dissolved in freshly distilled toluene (4 mL). The solution was refluxed for 32 h and then evaporated to dryness. ***Caution!*** *This reaction generates H_2 and should be carefully kept under nitrogen.* The addition of *n*-hexane to the reaction mixture afforded **1** as a spectroscopically pure solid (isolated yield 40.21 mg, 0.0468 mmol, 75%). Anal. Calcd for $Re_2C_{21}H_{12}O_8N_2S_2$: C, 29.44; H, 1.41; N, 3.27. Found: C, 29.45; H, 1.33; N, 3.50. IR (ν_{CO}, toluene): 2041m, 2021s, 1940s, 1917s cm^{-1}. ^{1}H NMR (400 MHz, CD_2Cl_2): δ 9.11 (d, 1H, Ha), 7.81 (d, 1H, Hb), 7.60 (dd, 1H, Hc), 7.19 (dd, 2H, Hα, thiophene ring), 7.10 (d, 1H, Hβ, thiophene), 7.07 (d, 1H, Hβ, thiophene), 4.52 (s, 1H), 2.92 (s, 3H, Me), −6.80 (s, 1H, hydride). GC (M = $[Re_2(\mu\text{-}H)(\mu\text{-}OOC\text{-}CPDT)(CO)_6(\mu\text{-}3\text{-}Me\text{-}pydz)]$, relative intensity): *m*/*z* 859 ([M]$^+$, 38), 858 ([M − H]$^+$, 36), 830 ([M − H − CO]$^+$, 100).

1′ was prepared from **2** and benzoic acid, using the same procedure as that described for **1**.[22] Anal. Calcd for $Re_2C_{18}H_{12}O_8N_2$: C, 28.57; H, 1.60; N, 3.70. Found: C, 28.77; H, 1.46; N, 3.43. IR (ν_{CO}, toluene): 2040m, 2020s, 1940s, 1913s cm^{-1}. ^{1}H NMR (400 MHz, CD_2Cl_2): δ 9.29 (d, 1H, Ha), 7.90 (d, 1H, Hb), 7.69 (dd, 1H, Hc), 7.93 (dd, 2H, H_o, phenyl), 7.38 (t, 2H, H_m, phenyl), 7.49 (t, 1H, H_p, phenyl), 3.06 (s, 3H, Me), −6.68 (s, 1H, hydride). GC (M = $[Re_2(\mu\text{-}H)(\mu\text{-}OOC\text{-}Ph)(CO)_6(\mu\text{-}3\text{-}Me\text{-}pydz)]$, relative intensity): *m*/*z* 759 ([M]$^+$, 24), 758 ([M − H]$^+$, 23), 730 ([M − H − CO]$^+$, 100).

Electrochemistry. Complex **1** (together with reference compounds CPDT-COOH and complex **1′**) was characterized by CV at potential scan rates ranging from 0.005 to 10 V s^{-1}, in 0.25 or 0.5 mM MeCN solutions, deaerated by N_2 purging, with different 0.1 M supporting electrolytes: $TBABF_4$ and $TBAPF_6$ (TBA = *n*-Bu_4N). The ohmic potential drop was compensated for by the positive feedback technique. The experiments were carried out using an AUTOLAB PGSTAT 12 potentiostat of EcoChemie (Utrecht, The Netherlands) run by a PC with the *GPES 4.9* software of the same manufacturer. The working electrode was either (i) a GC disk embedded in Teflon (Amel, 0.071 cm^2), (ii) a gold disk embedded in Teflon (Amel, 0.0314 cm^2), (iii) a platinum foil (1.44 cm^2) for bulk depositions, or (iv) an ITO-coated glass slide (Aldrich, sheet resistance 9−12 Ω sq^{-1}). The counter electrode was a platinum wire. The operating reference electrode was an aqueous saturated calomel electrode of a redox potential of −0.39 V in our MeCN working solutions versus that of the Fc^+/Fc couple (the intersolvental redox potential reference currently recommended by IUPAC).[41] The optimized polishing procedure for the working disk electrodes consisted of surface treatment with a synthetic diamond powder of 1 mm diameter from Aldrich on a DP-Nap wet cloth from Struers.

Electrochemical polymerization of **1** by repeated CV cycling in the potential range of the first anodic peak between −0.4 and 1.0 at a 0.2 V s^{-1} potential scan rate resulted in regular deposition of conducting films on the working electrodes. The CV stability of the films was tested by repeated cycling in the same potential range at different scan rates, in a monomer-free solution; finally, the potential range was progressively extended negatively in search of the first reduction potential and possible related charge-trapping phenomena.

The polymer growth was also monitored by electrochemical piezoelectric microgravimetry using an EQCM 5710 electrochemical quartz crystal microbalance (Institute of Physical Chemistry of the Polish Academy of Science) connected with the Autolab PGSTAT and run by *EQCM 5710-S2* software, depositing the polymer on gold-coated AT-cut quartz crystal resonators (5 MHz).

The mass variation was calculated according to Sauerbrey's equation:[42]

$$\Delta f = \frac{-2{f_0}^2 \Delta m}{A\sqrt{\mu_q \rho_q}}$$

where Δf = frequency change, Δm = mass variation, A = active piezogravimetric area = 0.1963 cm^2, ρ_q = quartz density = 2.648 g cm^{-3}, and μ_q = shear modulus of quartz = 2.947 × 10^{11} dyn cm^{-2}, under the assumption that the film density and shear modulus are the same as those of the quartz (an assumption reasonable for thin films with no compressive stress of mass <1% quartz crystal mass).

The film deposited on a GC electrode (20 cycles, MeCN with 0.1 M $TBAPF_6$) was also characterized in a monomer-free solution by EIS, using the above-described working cell and an AUTOLAB PGSTAT 302N (Metrohm Autolab) potentiostat equipped with a FRA2 module

dx.doi.org/10.1021/ic501840p | *Inorg. Chem.* 2014, 53, 11242−11251

(EcoChemie, Utrecht, The Netherlands), run by a PC with *NOVA* software of the same manufacturer. EIS spectra were recorded in the 10^5−10^{-2} Hz range polarizing the film at different potentials, from the neutral to the positively charged state.

Photophysical Measurements. Steady-state fluorescence measurements were performed with a Jobin-Yvon Fluorolog-3 spectrometer equipped with double monochromators and a Hamamatsu R928P photomultiplier tube as a detector, at room temperature. The solutions were prepared under dinitrogen by introducing quartz cuvettes into a suitable Schlenk tube and were deoxygenated by bubbling dinitrogen for 30 min before measurements. The emission intensities have been normalized to a nominal absorption value of 0.1. Quantum yields have been determined by a comparison with the emission of $[Ru(bpy)_3]Cl_2$ in deaerated acetonitrile (Φ = 0.062).[43]

Single-Crystal X-ray Diffraction Analysis. Crystal data for **1**: $C_{21}H_{12}N_2O_8Re_2S_2$, M_r = 856.85, monoclinic, space group $P2_1/n$ (No. 14), a = 10.625(2) Å, b = 20.994(2) Å, c = 11.677(2) Å, β = 105.00(2)°, V = 2515.9(7) Å^3, Z = 4, d_{calc} = 2.262 g cm^{-3}, T = 150(2) K, crystal size = 0.12 × 0.06 × 0.06 mm^3, μ = 9.827 mm^{-1}, λ(Mo Kα) = 0.71073 Å. Refinement of 303 parameters on 4431 independent reflections out of 35617 measured reflections (R_{int} = 0.1083, R_σ = 0.0624, and $2\theta_{max}$ = 50.0°) led to R_1 = 0.0429 [$I > 2\sigma(I)$], wR_2 = 0.0714 (all data), and S = 1.171, with the largest peak and hole of 1.060 and −1.440 e Å^{-3}. Details of data collection and structure solution and refinement can be found in the SI. CCDC 976867 contains the crystallographic data for **1**. These data can also be obtained free of charge from The Cambridge Crystallographic Data Centre.

Computational Details. Ground-state geometries were optimized by means of DFT calculations. The parameter-free hybrid functional PBE0[44] was employed along with the standard valence double-ζ polarized basis set 6-31G(d,p) for carbon, hydrogen, nitrogen, oxygen, and sulfur. For rhenium, the Stuttgart-Dresden effective core potentials were employed along with the corresponding valence triple-ζ basis set. The nature of all of the stationary points was checked by computing vibrational frequencies. In order to simulate the absorption electronic spectrum down to 250 nm, the lowest 30 singlet excitation energies were computed by means of TD-DFT calculations. Calculations were done also in the presence of solvent (dichloromethane), described by the polarizable continuum model using the integral equation formalism.[45] All of the calculations were done with *Gaussian 09*.[46]

■ ASSOCIATED CONTENT

Ⓢ Supporting Information

X-ray crystallographic data of complex **1** in CIF format and details on the electrochemical, spectroscopic, crystallographic, and computational characterization. This material is available free of charge via the Internet at http://pubs.acs.org.

■ AUTHOR INFORMATION

Corresponding Authors

* E-mail: monica.panigati@unimi.it. Phone: +390250314352. Fax: +390250314405.
*E-mail: pierluigi.mercandelli@unimi.it. Phone: +390250314447. Fax: +390250314454.
*E-mail: patrizia.mussini@unimi.it. Phone: +390250314211. Fax: +390250314405.

Notes

The authors declare no competing financial interest.

■ ACKNOWLEDGMENTS

M.P., P.M., and G.D. thank the Italian Ministero dell'Istruzione, Università e Ricerca, for financial support (Grants PRIN-2009PRAM8L and PRIN-2012A4Z2RY).

■ REFERENCES

(1) (a) Robinson, K. L.; Lawrence, N. S. *Anal. Chem.* **2006**, *78*, 2450−2455. (b) Wang, Z.; McWilliams, A. R.; Evans, C. E. B.; Lu, X.; Chung, S.; Winnik, M. A.; Manners, I. *Adv. Funct. Mater.* **2002**, *12*, 415−419. (c) Payne, S. J.; Fiore, G. L.; Fraser, C. L.; Demas, J. N. *Anal. Chem.* **2010**, *82*, 917−921. (d) Holliday, B. J.; Stanford, T. B.; Swager, T. M. *Chem. Mater.* **2006**, *18*, 5649−5651.
(2) (a) Collot, J.; Gradinaru, J.; Humbert, N.; Skander, M.; Zocchi, A.; Ward, T. R. *J. Am. Chem. Soc.* **2003**, *125*, 9030−9031. (b) Cecchet, F.; Alebbi, M.; Bignozzi, C. A.; Paolucci, F. *Inorg. Chim. Acta* **2006**, *359*, 3871−3874.
(3) (a) Wong, W.-Y.; Ho, C.-L. *Acc. Chem. Res.* **2010**, *43*, 1246−1256. (b) Wong, W.-Y.; Wang, X.-Z.; He, Z.; Djurišić, A. B.; Yip, C.-T.; Cheung, K.-Y.; Wang, H.; Mak, C. S. H.; Chan, W.-K. *Nat. Mater.* **2007**, *6*, 521−527.
(4) Ulbricht, C.; Remzi Becer, C.; Winter, A.; Schubert, U. S. *Macromol. Rapid Commun.* **2010**, *31*, 827−833.
(5) Choi, T.-L.; Lee, K.-H.; Joo, W.-J.; Lee, S.; Lee, T.-W.; Chae, M. Y. *J. Am. Chem. Soc.* **2007**, *129*, 9842−9843.
(6) Monk, P. M. S.; Mortimer, R. J.; Rosseinsky, D. R. *Electrochromism: Fundamentals and Applications*; VCH: Weinheim, Germany, 1995.
(7) (a) Manners, I. *Synthetic Metal-Containing Polymers*; Wiley-VCH: Weinheim, Germany, 2004. (b) Nguyen, P.; Gomez-Elipe, P.; Manners, I. *Chem. Rev.* **1999**, *99*, 1515−1548. (c) Manners, I. *Science* **2001**, *294*, 1664−1666. (d) Schubert, U. S.; Eschbaumer, C. *Angew. Chem., Int. Ed.* **2002**, *41*, 2892−2926. (e) Wolf, M. O. *Adv. Mater.* **2001**, *13*, 545−553. (f) Roncali, J. *J. Mater. Chem.* **1999**, *9*, 1875−1893. (g) Wolf, M. O.; Zhu, Y. *Adv. Mater.* **2000**, *12*, 599−601. (h) Kingsborough, R. P.; Swager, T. M. Transition Metals in Polymeric π-Conjugated Organic Frameworks. In *Progress in Inorganic Chemistry*; Karlin, K. D., Ed.; John Wiley & Sons: Hoboken, NJ, 1999; Vol. *48*, pp 123−231. (i) Pickup, P. G. *J. Mater. Chem.* **1999**, *9*, 1641−1653. (j) Stott, T. L.; Wolf, M. O. *Coord. Chem. Rev.* **2003**, *246*, 89−101. (k) Zhou, J.; Whittell, G. R.; Manners, I. *Macromolecules* **2014**, *47*, 3529−3543. (l) Wolf, M. O. Synthesis and Properties of Oligo- and Polythiophenes Containing Transition Metals. In *Handbook of Thiophene-Based Materials*; Perepichka, I. F., Perepichka, D. F., Eds.; John Wiley & Sons: Hoboken, NJ, 2009; pp 293−319.
(8) Whittell, G.; Hager, M. D.; Schubert, U. S.; Manners, I. *Nat. Mater.* **2011**, *11*, 176−188.
(9) Holliday, B. J.; Swager, T. M. *Chem. Commun.* **2005**, 23−36.
(10) Heinze, J.; Frontana-Uribe, B. A.; Ludwigs, S. *Chem. Rev.* **2010**, *110*, 4724−4771.
(11) (a) Kang, B. S.; Kim, D. H.; Jung, T. S.; Jang, E. K.; Pak, Y.; Shin, S. C.; Park, D.-S.; Shim, Y.-B. *Synth. Met.* **1999**, *105*, 9−12. (b) Kim, D. H.; Park, D.-S.; Shim, Y.-B.; Shin, S. C. *J. Organomet. Chem.* **2000**, *608*, 133−138. (c) Kim, D. H.; Kim, J.-H.; Kim, T. H.; Kang, D. M.; Kim, Y. H.; Shim, Y.-B.; Shin, S. C. *Chem. Mater.* **2003**, *15*, 825−827.
(12) Coppo, P.; Turner, M. L. *J. Mater. Chem.* **2005**, *15*, 1123−1133.
(13) Zotti, G.; Zecchin, S.; Schiavon, G.; Berlin, A.; Pagani, G.; Canavesi, A. *Chem. Mater.* **1995**, *7*, 2309−2315.
(14) Schmittel, M.; Lin, H. *J. Mater. Chem.* **2008**, *18*, 333−343.
(15) Donghi, D.; D'Alfonso, G.; Mauro, M.; Panigati, M.; Mercandelli, P.; Sironi, A.; Mussini, P.; D'Alfonso, L. *Inorg. Chem.* **2008**, *47*, 4243−4255.
(16) Panigati, M.; Donghi, D.; D'Alfonso, G.; Mercandelli, P.; Sironi, A.; D'Alfonso, L. *Inorg. Chem.* **2006**, *45*, 10909−10921.
(17) Raimondi, A.; Panigati, M.; Maggioni, D.; D'Alfonso, L.; Mercandelli, P.; Mussini, P.; D'Alfonso, G. *Inorg. Chem.* **2012**, *51*, 2966−2975.
(18) Panigati, M.; Mauro, M.; Donghi, D.; Mercandelli, P.; Mussini, P.; De Cola, L.; D'Alfonso, G. *Coord. Chem. Rev.* **2012**, *256*, 1621−1643.
(19) Mauro, M.; Quartapelle Procopio, E.; Sun, Y.; Chien, C.-H.; Donghi, D.; Panigati, M.; Mercandelli, P.; Mussini, P.; D'Alfonso, G.; De Cola, L. *Adv. Funct. Mater.* **2009**, *19*, 2607−2614.

(20) Mauro, M.; Yang, C.-H.; Shin, C.-Y.; Panigati, M.; Chang, C.-H.; D'Alfonso, G.; De Cola, L. *Adv. Mater.* **2012**, *24*, 2054−2058.
(21) Berlin, A.; Zotti, G.; Schiavon, G.; Zecchin, S. *J. Am. Chem. Soc.* **1998**, *120*, 13453−13460.
(22) Panigati, M.; Quartapelle Procopio, E.; Mussini, P. To be published.
(23) Tacca, A.; Po, R.; Caldararo, M.; Chiaberge, S.; Gila, L.; Longo, L.; Mussini, P.; Pellegrino, A.; Perin, N.; Salvalaggio, M.; Savoini, A.; Spera, S. *Electrochim. Acta* **2011**, *56*, 6638−6653.
(24) The atomic spin-density population computed for the more stable conformation of the radical cation $\mathbf{1}^+$ shows that the unpaired electron is mainly delocalized over the terminal α position of the two thiophene rings (0.72 e) and, to a lesser extent, over the four sp^2-hybridized carbon atoms of the cyclopentadiene core (0.20 and 0.44 e for the atoms next to sulfur and next to the sp^3 carbon, respectively), and over the β-terminal position of the two thiophene rings (−0.22 e), with a minimal contribution from the sulfur atom (−0.10 e; all of the values are sums over equivalent positions). As expected, the unpaired electron in the radical cation is distributed over the molecule in accordance with the composition of the HOMO (depicted in Figure 2).
(25) (a) Casalbore-Miceli, G.; Camaioni, N.; Geri, A.; Cristani, M.; Fichera, A. M.; Berlin, A. *Synth. Met.* **2000**, *108*, 47−56. (b) Casalbore-Miceli, G.; Camaioni, N.; Geri, A.; Berlin, A.; Campesato, R. *Electrochim. Acta* **1999**, *44*, 4781−4786.
(26) (a) Zotti, G.; Schiavon, G.; Berlin, A.; Fontana, G.; Pagani, G. *Macromolcules* **1994**, *27*, 1938−1942. (b) Camaioni, N.; Casalbore-Miceli, G.; Beggiato, G.; Cristiani, M.; Summonte, C. *Thin Solid Films* **2000**, *366*, 211−215.
(27) In the literature, the first reduction peak of poly-CPDT is located at about −2.6 V (Fc^+/Fc). Zotti, G.; Zecchin, S.; Schiavon, G.; Berlin, A. *Macromolecules* **2001**, *34*, 3889−3895.
(28) Charge trapping has never been observed for the polymer obtained from the free ligand CPDT-COOH (see Figure S9 in the SI).
(29) Casalbore-Miceli, G.; Camaioni, N.; Geri, A.; Ridolfi, G.; Zanelli, A.; Gallazzi, M. C.; Maggini, M.; Benincori, T. *J. Electroanal. Chem.* **2007**, *603*, 227−234 and references cited therein.
(30) Casalbore-Miceli, G.; Gallazzi, M. C.; Zecchin, S.; Camaioni, N.; Geri, A.; Bertarelli, C. *Adv. Funct. Mater.* **2003**, *13*, 307−312.
(31) (a) Zotti, G.; Schiavon, G.; Zecchin, S. *Synth. Met.* **1995**, *72*, 275−281. (b) Denisevich, P.; Willman, K. W.; Murray, R. W. *J. Am. Chem. Soc.* **1981**, *103*, 4727−4737.
(32) Denisovich, P.; Abruna, H. D.; Leidner, C. R.; Meyer, T. J.; Murray, R. W. *Inorg. Chem.* **1982**, *21*, 2153−2161.
(33) Musiani, M. *Electrochim. Acta* **1990**, *35*, 1665−1670.
(34) Lasia, A. Electrochemical Impedance Spectroscopy and Its Applications. In *Modern Aspects of Electrochemistry*; Conway, B. E., Bockris, J. O'M., White, R. E., Eds.; Kluwer Academic/Plenum Publishers: New York, 1999; Vol. *32*, pp 143−248.
(35) Zotti, G.; Schiavon, G.; Zecchin, S.; Berlin, A.; Pagani, G.; Canavesi, A. *Langmuir* **1997**, *13*, 2694−2698.
(36) (a) Conil, J.; Brédas, J. L. *Adv. Mater.* **1995**, *7*, 295−297. (b) Sakai, T.; Satou, T.; Kaikawa, T.; Takimiya, K.; Otsubo, T.; Aso, Y. *J. Am. Chem. Soc.* **2005**, *127*, 8082−8089. (c) Klod, S.; Haubner, K.; Jähne, E.; Dunsch, L. *Chem. Sci.* **2010**, *1*, 743−750.
(37) (a) Hill, M. G.; Penneau, J. F.; Zinger, B.; Mann, K. R.; Miller, L. L. *Chem. Mater.* **1992**, *4*, 1106−1113. (b) Yu, Y.; Gunic, E.; Zinger, B.; Miller, L. L. *J. Am. Chem. Soc.* **1996**, *118*, 1013−1018. (c) Hill, M. G.; Mann, K. R.; Miller, L. L.; Penneau, J.-F. *J. Am. Chem. Soc.* **1992**, *114*, 2728−2730. (d) Capel Ferrón, C.; Capdevila-Cortada, M.; Balster, R.; Hartl, F.; Niu, W.; He, M.; Novoa, J. J.; López Navarrete, J. T.; Hernández, V.; Ruiz Delgado, M. C. *Chem.—Eur. J.* **2014**, *20*, 10351−10359.
(38) Valenti, G.; Panigati, M.; Boni, A.; D'Alfonso, G.; Paolucci, F.; Prodi, L. *Inorg. Chim. Acta* **2014**, *417*, 270−273.
(39) Benincori, T.; Brenna, E.; Sannicolò, F.; Trimarco, L.; Moro, G.; Pitea, D.; Pilati, T.; Zerbi, G.; Zotti, G. *J. Chem. Soc., Chem. Commun.* **1995**, 881−882.
(40) Jeffries, A. T.; Moore, K. C.; Ondeyka, K. D. M.; Springsteen, A. W.; MacDowell, D. W. H. *J. Org. Chem.* **1981**, *46*, 2885−2889.
(41) Gritzner, G.; Kuta, J. *Pure Appl. Chem.* **1984**, *56*, 461−466.
(42) Buck, R. P.; Lindner, E.; Kutner, W.; Inzelt, G. *Pure Appl. Chem.* **2004**, *76*, 1139−1160.
(43) Ishida, A.; Tobita, S.; Hasegawa, Y.; Katoh, R.; Nozaki, K. *Coord. Chem. Rev.* **2010**, *254*, 2449−2458.
(44) Called PBE1PBE in Gaussian. (a) Adamo, C.; Barone, V. *J. Chem. Phys.* **1999**, *111*, 6158−6170. (b) Perdew, J. P.; Burke, K.; Ernzerhof, M. *Phys. Rev. Lett.* **1996**, *77*, 3865−3868. (c) Perdew, J. P.; Burke, K.; Ernzerhof, M. *Phys. Rev. Lett.* **1997**, *78*, 1396.
(45) Tomasi, J.; Mennucci, B.; Cammi, R. *Chem. Rev.* **2005**, *105*, 2999−3093.
(46) *Gaussian 09*, revision C.01; Gaussian Inc.: Wallingford, CT, 2004.